Exploring Abeta42 Monomer Diffusive Dynamics on Fibril Surfaces through Molecular Simulations

Yuan-Wei Ma[1,2], Guan-Fang Wang[2], and Min-Yeh Tsai[2,3*]

[1]*Institute of Bioinformatics and Structural Biology, National Tsing-Hua University, Hsinchu, 300044, Taiwan*

[2]*Department of Chemistry and Biochemistry, National Chung Cheng University, Minhsiung, Chiayi 621301, Taiwan*

[3]*Division of Physics, National Center for Theoretical Sciences, National Taiwan University, Taipei 106319, Taiwan*

**Corresponding author: Min-Yeh Tsai, Department of Chemistry and Biochemistry, National Chung Cheng University, Minhsiung, Chiayi, Taiwan, myt@ccu.edu.tw*

Feb 29th, 2024

Abstract

Alzheimer's disease is closely linked to the aggregation of Abeta42 peptides, which follow a complex pathway involving primary nucleation and secondary processes. While previous research has underscored the importance of secondary processes, this study employs molecular dynamics simulations to delve into their molecular-level intricacies. We employ coarse-grained molecular dynamics with a freely diffusing Abeta42 monomer alongside a pre-formed fibril structure. We conducted comprehensive calculations of the monomer's diffusion coefficient (D) on the fibril surface, considering both straight and twisted fibril structures, as well as various monomer surface orientations. Notably, our findings reveal a robust correlation between the monomer's diffusion coefficient (D) and its surface orientation, irrespective of the degree of fibrillar twisting. Additional analysis of monomer orientation further reinforces the orientation-dependent diffusion results, distinguishing between parallel and perpendicular alignments. Additionally, we explore how distinct fibril surfaces influence monomer dynamics. We compared the C-terminal and N-terminal surfaces

and found that the monomer exhibits lower diffusion coefficients (D) on the N-terminal surface. Surface roughness, quantified using root-mean-square deviation (RMSD), revealed significant differences between these surfaces. The dissimilarity in shape and roughness contributes to the observed differences in monomer dynamics, highlighting the role of surface characteristics in molecular-level aggregation.

1 INTRODUCTION

Protein aggregation plays a pivotal role in diseases such as Alzheimer's, especially in the context of the Amyloid Hypothesis.[1] Understanding this process, which includes nucleation, fibril growth, and breakage, is crucial for developing potential therapeutic interventions.[2] Despite this, the treatment landscape for Alzheimer's faces significant challenges. This is evident in the case of FDA-approved drugs like Aducanumab (Aduhelm), which are limited by usage constraints and safety issues.[3,4]

Recent studies propose the 'oligomer hypothesis,' suggesting that amyloid fibers may represent thermodynamic end-products while toxic elements arise from oligomers formed during protein aggregation[5–7] (also refer to a recent comprehensive review[8]). Understanding primary nucleation mechanisms in amyloid fibers is well-established,[9–11] yet the dynamic complexity of protein aggregation, especially at lower concentrations (<10μM), remains critical. Secondary processes like filament breakage and secondary nucleation further complicate our comprehension, impacting neurodegenerative disease progression.[12,13]

The interplay of fibril growth and secondary processes is intricately linked to interactions at fibril surfaces and subsequent catalytic properties. Despite pioneering experiments elucidating surface-mediated nucleation (for example, sickle hemoglobin[14,15] and amyloid proteins[13,16]), a significant knowledge gap persists in understanding the molecular mechanisms underpinning these processes. These processes are crucial as they significantly influence the formation of toxic oligomers,[17–19] reflect reactive surface binding sites,[18,20] and modulate the macroscopic 'lag time'.[17] This gap is particularly evident in the limited experimental data available for visualizing these interactions in real-time or at atomic resolution, as emphasized in recent reviews.[21] Computational simulations serve as a powerful tool in bridging this gap, offering valuable insights into molecular interactions that are difficult to capture experimentally.[21,22]

Full-atom simulations have shed light on early structural changes in aggregation, particularly hydrophobic and electrostatic forces influencing peptide adsorption on surfaces.[23,24] Coarse-grained models better explore longer timescales and biological contexts, revealing multiple aggregation pathways influenced by peptide-surface interactions and rigidity.[25–29]

Studies emphasize protein monomer mobility and lateral diffusion on surfaces in surface-mediated protein aggregation.[30–33] A crucial aspect of this is the intricate balance in the energy of protein monomer-surface interactions, which lies within a very narrow range and fulfills the energy requirement for secondary nucleation.[34] However, our understanding of monomer conformations and their diffusion behavior at the microdynamic level is still incomplete. For instance, the relationship between a protein's conformation and its diffusion dynamics on fibril surfaces remains an intriguing question. Gaining a comprehensive insight into these aspects is essential for effectively controlling monomer dynamics on surfaces.

Understanding the dynamics of protein monomers on fibril surfaces is not just crucial for surface-mediated aggregation, but also connects to broader principles in physical science. This leads us to consider the fundamental role of diffusion in natural processes, a concept central to the fluctuation-dissipation theory.[35] Diffusion, a key driver of atomic and molecular Brownian motion, manifests across various states of matter, including gases, liquids, solids, and glasses. Within biological contexts, such as in protein behavior, we observe significant variability in diffusion rates contingent on the environment. For example, protein diffusion is markedly slower in the crowded cytoplasm compared to dilute solutions (10 $\mu m^2/s$ vs. 100 $\mu m^2/s$).[36] Specifically, when proteins are attached to fibril surfaces, advanced techniques like Total Internal Reflection Fluorescence Microscopy (TIRFM) and Atomic Fluorescence Microscopy (AFM) have been instrumental in estimating diffusion coefficients, which range between 0.5-2.4 $\mu m^2/s$.[32]

Our study centers on the 'Amyloid Cascade Hypothesis' for protein aggregation where the mechanisms of seeded polymerization and surface-catalyzed nucleation are hypothesized to be crucial for the development and progression of these amyloid plaques. These processes suggest that secondary processes on fibril surfaces depend on the dynamics and structure of newly attached protein monomers. Heterogeneous fibril surfaces, including assembly defects and specific amino acid binding sites, facilitate monomer diffusion, sliding, collisions, secondary nucleation, fibril elongation, and breakage, possibly leading to toxic aggregates. To explore this, we employ the openAWSEM simulation platform,[37] known for its accuracy in physicochemical information, biological self-assembly, and fibril aggregation studies.[38–41] openAWSEM excels in biophysical mesoscale kinetic analysis, capturing relevant time scales and molecular details, making it ideal for investigating the mesoscopic diffusion dynamics of amyloid-like peptides on fibril surfaces, a pioneering endeavor in this field.

By leveraging extensive simulations guided by energy landscape theory, the goal is to unravel the role of surface interactions in governing fibril growth, potentially offering innovative insights for neurodegenerative disease treatment and management. This research aims to enrich theoretical understanding and guide experimental approaches in this vital field of study.

2 METHODS

2.1 Open Associative-memory, water-mediated, structure and energy model (OpenAWSEM)

In this study, openAWSEM is employed—a python implementation of the AWSEM protein coarse-grained force field devised by Wolynes and colleagues, as outlined by Lu et al.[37] This innovative simulation framework is constructed on openMM[42] to fulfill a rapid (GPU-enabled), adaptable, and user-friendly purpose. OpenAWSEM follows the legacy of the Associative-memory, Water-mediated, Structure and Energy Model (AWSEM) for molecular dynamics (MD) simulation, as introduced by Davtyan et al.[43]

Within the AWSEM framework, each amino acid residue is denoted by three atoms: C_α, C_β, and O (with glycine being an exception). The physicochemical characteristics of diverse side chains manifest in the C_β atoms. The AWSEM-MD simulation protocol has found applications in addressing a spectrum of biological inquiries, encompassing protein structure prediction,[43–46] prognostication of protein binding events,[44] investigation of protein aggregation phenomena,[47,48] and exploration of intricate protein-DNA assemblies and remodeling processes.[49–52] Prospective readers are invited to explore the online web-server variant, AWSEM-Suite, designed for structure prediction.[53]

2.2 Structural preparation and simulation protocol for Abeta monomer attaching fibrils

We use the CreateFibril2.5[54] to construct the 62 chain fibril with PDB ID:2MXU topology. The simulation of amyloid fibril is performed using the "CreateFibril2.5" tool, which replicates and extends selected protein chains from a specified PDB file. This process involves setting various parameters to control the replication, rotation, and placement of monomers along the fibril axis.

To initiate the simulation, the input filename (PDB file) is specified using the "-f" parameter (e.g., python CreateFibril.py -f 2MXU.pdb). Following this, the "-c" parameter is employed to select the chains to be replicated and extended; for instance, -c 2,3 designates chains B and C for replication. Subsequently, the "-r" parameter dictates the number of replications for the chosen chains (e.g., -r 30 replicates chains B and C 30 times). The rotation angle of monomers during aggregation is controlled by the "-a" parameter, with -a 0 indicating no rotation. To define the structural characteristics, the total number of residues (amino acids) in the protein is set using the "-nr" parameter (e.g., -nr 32 for a protein with 32 residues). The coordinates and residue point where the fibril axis passes are specified through the "-fp" parameter (e.g., -fp -0.062,-7.195,14.462,26).

Executing the complete command integrates all specified parameters (e.g., python CreateFibril.py -f 2MXU.pdb -c 2,3 -r 30 -a 0 -fp -0.062,-7.195,14.462,26 -nr 32), resulting in the generation of a simulated amyloid fibril with extended protein chains, controlled rotation angles, and defined fibril axis coordinates. Figure 1 presents the filamentous model generated using the tool. We plan to use this model to study diffusion of a monomer along the fibrl surface.

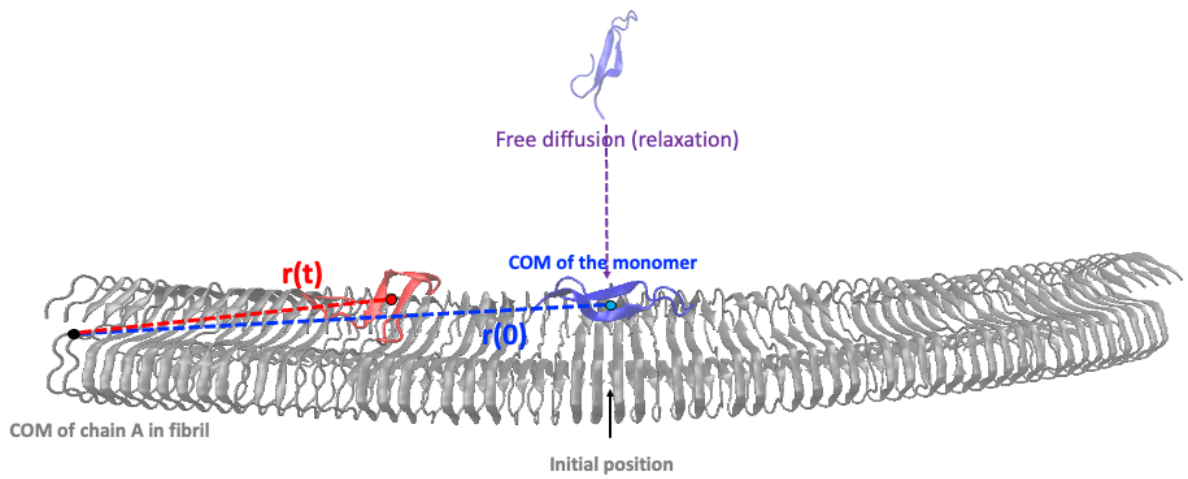

Figure 1. Schematic diagram illustrating the simulation of Abeta monomer diffusion along fibril surfaces, including free diffusion scenarios.

The simulation features a long fibril filament comprising 62 chains (shown in gray cartoon representation) and an additional Abeta monomer. The monomer is depicted under three distinct scenarios: 1) Initially detached from the fibril and shown in transparent blue. 2) At position $r(0)$, illustrating its first point of attachment to the fibril, highlighted in blue. 3) At position $r(t)$, representing its location at time t, shown in red. The position vector, r, is defined with the reference point being the center-of-mass of chain A (the leftmost chain) in the fibril.

2.3 Nematic Order Parameter

To delineate the distinction in structure among fibril polymorphs, we utilized the nematic order parameter (P2 value) to quantify the structured arrangement on the surface of fibrils. Initially devised for delineating structural order in liquid crystals, the nematic order parameter found its introduction in the investigation of protein aggregation by Caflisch and colleagues.[55] Subsequently, this parameter was employed to elucidate aggregation of Amyloid-beta fibrils[38,56,57] and has recently undergone comparison with order parameters acquired through neural network learning, as demonstrated by Charest et al.[58]

2.4 Mean Square Displacement

We use mean square displacement (MSD) formula to calculate the diffusion coefficient (D), as shown below.

$$\mathrm{MSD}(t) = \langle |\mathbf{r}(t) - \mathbf{r}(0)|^2 \rangle = \frac{1}{N} \sum_{i=1}^{N} |\mathbf{r}_i(t) - \mathbf{r}_i(0)|^2 \tag{1}$$

$$\lim_{t \to \infty} \langle |\mathbf{r}(t) - \mathbf{r}(0)|^2 \rangle = 2Dt \tag{2}$$

where t refers to time; r(0) represents the initial Center-of-Mass (COM) distance between the monomer and the chain A in the fibril; r(t) is the COM distance between the monomer and the chain A in the fibril changes over time.

2.5 Importance sampling and free energy analysis

The computation of free energy, specifically the potential of mean force (PMF), is executed utilizing the pyEMMA python package, developed by Noe and collaborators (Scherer et al., 2015). When calculating PMFs, a specific progress coordinate must be chosen for sampling. Due to the challenging accessibility of high-energy configuration space through thermal activation alone, a biasing force becomes necessary to guide the sampling towards the desired configurational space—a process referred to as "importance sampling."

In practical application, as with previous studies, all sampling tasks were conducted through molecular dynamics simulations on the openAWSEM platform.[38] To trace the trajectory of a monomer diffusing towards a specified position on the fibril's surface, numerous sampling windows were prepared. Diverse sampling windows were established by applying a series of harmonic biasing restraints between the centers of mass (one from the monomer and the other from the even-end of the fibril). These restraints were centered at distances ranging from 20 to 230 Å (with an interval of approximately 2.2 Å) from the even-end (chain A) in the fibril, with the monomer located on the surface. A total of 110 independent simulations were generated as a result.

The biasing coordinate is defined as the center of mass distance between the monomer and chain A in the fibril, with a biasing force constant (k) set at 6 kcal/mol (25 kJ/mol) for all 110 simulations. Each simulation runs for 5 million time steps, with 5,000 frames outputted for analysis (every 1,000 time steps). We further utilized a stride of 100 to make 5000 to 50 frames for each window. Subsequently, data collected from the simulation trajectories (across 110 sampling windows) were reweighted using the WHAM technique,[59] implemented in the pyEMMA package (thermo.wham).[60] The distribution of all sampling windows is presented in the Supporting Information.

2.6 Root Mean Square Distance / Surface Roughness (S_R value)

We intend to define different surface properties with their shape or roughness. Specifically, we caculate the RMSD of CA atoms against an optimized surface plane. The centroid, representing the geometric center, is computed based on the alpha carbon (CA) atoms of residues 1 to 16 coordinates (N-ter) or 36 to 42 (C-ter surface). The covariance matrix is then computed from the coordinates, providing a measure of the interdependence of atom positions. Eigenvalue decomposition is applied to the covariance matrix, facilitating the extraction of eigenvalues and eigenvectors. The plane equation coefficients ($ax + by + cz + d = 0$) are derived from the eigenvector corresponding to the smallest eigenvalue, defining the plane in three-dimensional space. The RMSD is determined concerning the plane. The selected atoms for this calculation are the CA atoms of residues 1 to 16 (N-ter) or 36 to 42 (C-ter surface). The RMSD is calculated based on the root mean square distances of between CA atoms and the plane, providing a measure of structural deviation from the plane, termed surface roughness (S_R value).

3 RESULTS

3.1 Differential Diffusive Behaviors of Abeta Monomers Based on Orientation on Fibril Surface

Figure 2 illustrates a key discovery: monomers on the C-terminal fibril surface exhibit two distinct orientations – parallel and orthogonal (shown in Figure 2A). The Mean Squared Displacement (MSD) graph, plotted over time, provides valuable insights into this diffusion phenomenon. By analyzing the slope of this graph, we determine the diffusion coefficient, revealing that the orientation of the monomer significantly influences surface dynamics. Specifically, our results indicate that monomers oriented parallel to the fibril main axis diffuse faster, exhibiting a larger diffusion coefficient, compared to those oriented orthogonally (illustrated in Figure 2B). To further investigate the impact of monomer orientation on the diffusion process, we utilized the P2 order parameter. This approach helps quantify the distinction between the orientations. Figure 2C shows two lines corresponding to the two orientations, demonstrating that the orthogonal monomers have a higher order on the surface than the parallel ones throughout the trajectory. Additionally, Figure 4D presents the averaged P2 value over this trajectory, offering a comprehensive view of the orientation dynamics.

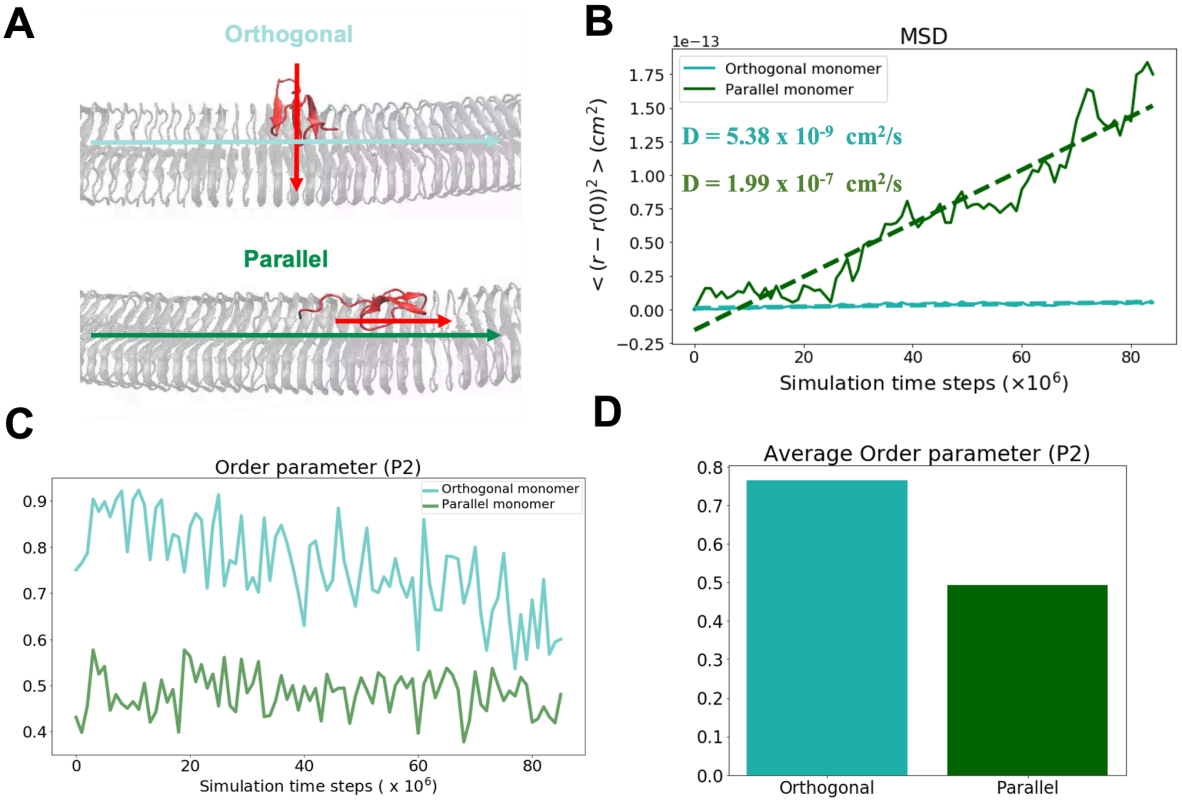

Figure 2. The orientation of an Abeta42 monomer on the fibril surface, along with tis diffusive dynamics, are analyzed. (A) Schematic diagram illustrating the two main orientation parallel/orthogonal of the monomer on the fibril surface. (B) Mean-squared-displacement (MSD) over time. Diffusion coefficient is derived from the MSD. (C) The order parameter (P2) of the different orientation monomer on the fibril surface changes over simulation time steps. (D) The average order parameter P2 is compared. Orthogonal monomer is labeled in light green. Parallel monomer is labeled in dark green.

3.2 Unveiling Asymmetry in Fibril Growth: Computational Insights into Surface Binding Affinities

Our study delves into the fibril surface binding affinities and their position-dependent characteristics to better understand the mechanism of fibril growth kinetics. Using umbrella sampling, we explored the free energy landscape of monomers on the C-terminal surface. We

observed a notable decrease in free energy as the monomer approaches a specific end, indicating a preference for binding to the even end over the odd end (illustrated in Figure 3). This observation aligns with the findings of a recent experimental study by Dev Thacker et al. (refer to Figure 5 in their publication)[61], which reported asymmetric growth at the fiber endpoints. Our computational results not only corroborate this experimental evidence of fibril asymmetry but also provide a deeper computational insight into it. This discovery is crucial as it sheds light on the intricate mechanics of fibril growth, offering a clearer understanding of the underlying processes that govern this phenomenon.

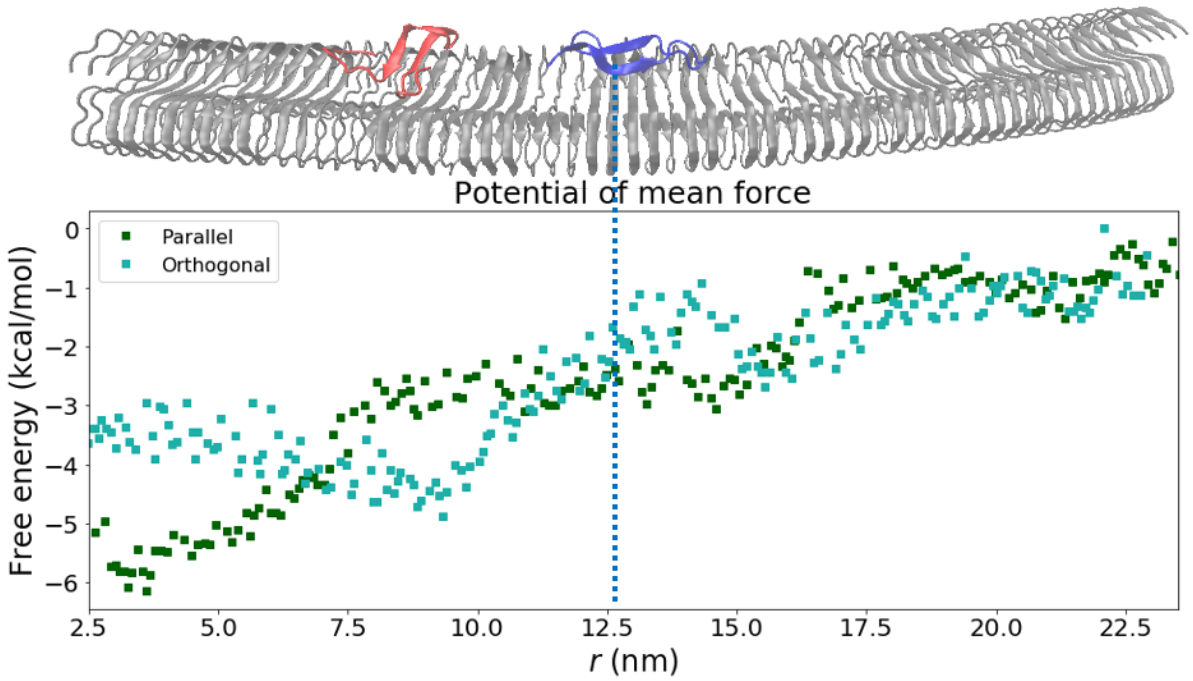

Figure 3. Free energy profile of the parallel monomer on the C-ter fibril surface. The free energy of a parallel monomer on the C-ter surface is the blue line. The free energy of an orthogonal monomer on the C-ter surface is the blue line.

3.3 Quantitative Surface Roughness Analysis Clarifies Differences Between N-terminal and C-terminal Surfaces

We conducted a comparative analysis of different surface properties on the same fiber, with a specific focus on the C-terminal (C-ter) and N-terminal (N-ter) surfaces, as shown in Figure 4A. Our observations revealed that when monomers with a parallel orientation interact with the N-ter surface, their diffusion coefficient (D) tends to be smaller compared to their interaction on the C-ter surface. This suggests reduced dynamics on the N-ter surface, as depicted in Figure 4C.

Interestingly, despite the monomers exhibiting similar parallel orientations on both C-ter and N-ter surfaces, there is a noticeable difference in their P2 quantified properties. Specifically, monomers on the N-ter surface show a lower order compared to those on the C-ter surface. We hypothesize that this variation stems from the distinct shapes of the N-ter and C-ter surfaces, influencing the P2 values.

Our analysis extended beyond the P2 properties of the monomers to a deeper examination of the structural differences between the N-ter and C-ter surfaces. Structurally, the C-ter surface is smoother, offering a more favorable landing area for monomers, whereas the N-ter surface is comparatively rougher. To quantify this, we employed the average Root Mean Square (RMS) Distance, measuring the fluctuations in distance between atoms and the best-fit plane, which is defined by a normal vector corresponding to the smallest eigenvalue (termed as the Surface Roughness (S_R) value). Conceptually, a higher RMS Distance indicates greater surface roughness due to increased fluctuations. Our RMSD analysis confirmed that the N-ter surface is indeed rougher than the C-ter surface, as illustrated in Figure 4D. In conclusion, our findings suggest that the surface shape not only influences the monomer's orientation but also entraps it in a state of reduced diffusive dynamics.

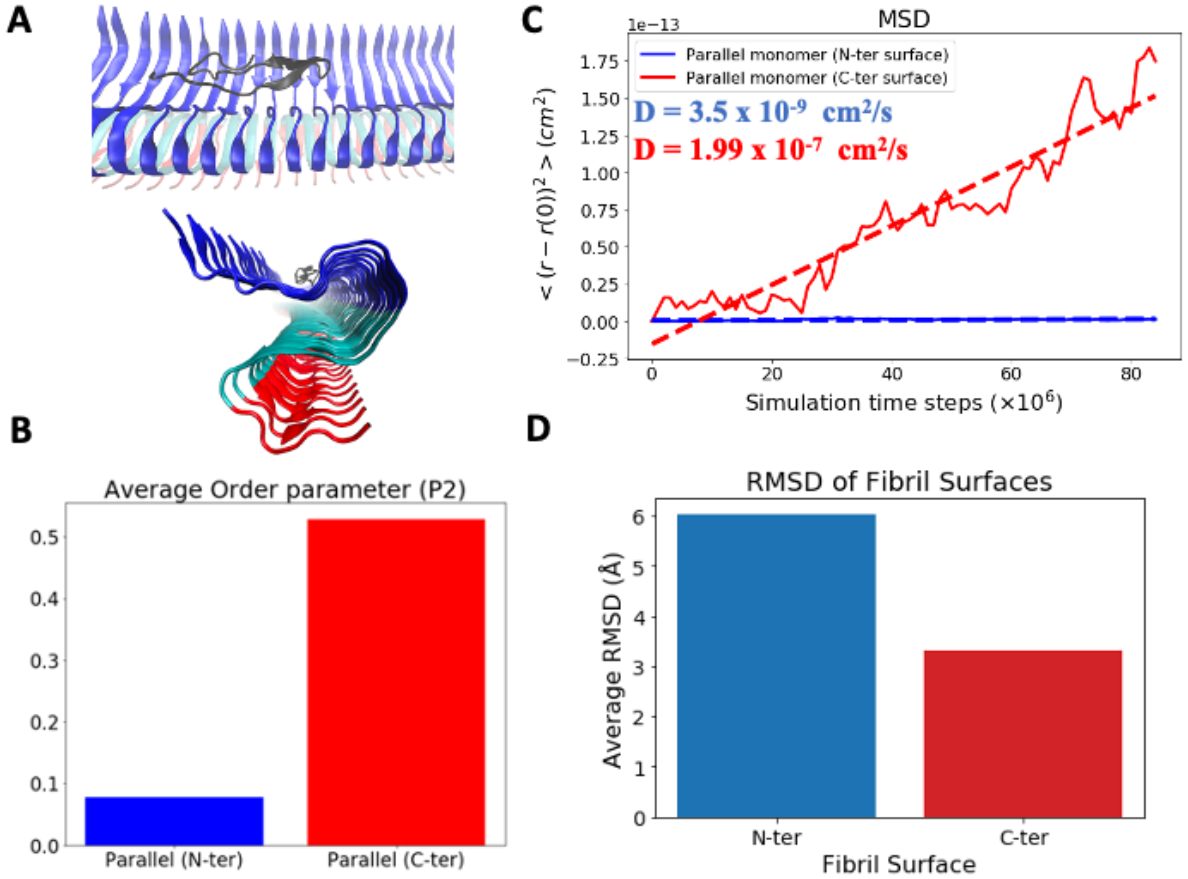

Figure 4. Distinct different fibril surfaces display different diffusive behaviors. (A) Structure diagram of 61 chains fibril. Red region represents the C-terminal surface. Blue region represents the N-terminal surface. Black indicates the monomer lies on the N-ter surface (B) Average P2 of the monomer lies on the N-ter (blue)/ C-ter (red) surface. (C) The MSD of the monomer lies on the C-ter surface (Red line). The MSD of the monomer lies on the N-ter surface (Blue line). (D) Average RMS Distance of the N-ter (blue) / C-ter (red) surface.

4 DISCUSSIONS

Monomer Orientation's Active Role in Fibril Growth

It is suggested that the fibril surface contributes actively to fibril growth, rather than serving merely as a passive scaffold.[61,62] This perspective offers a nuanced understanding of amyloid protein dynamics on pre-existing fibrils, an area critical for advancing our approach to neurodegenerative diseases [Citation]. Investigations using [method] have revealed how alterations in protein dynamics on fibrils correlate with the progression of diseases like Alzheimer's [describe findings].

Deviations in these dynamic processes could lead to abnormal fibril growth and morphology, potentially culminating in cellular toxicity [Citation]. Observational studies using techniques like [specific microscopy or imaging technique] have documented how variations in diffusion contribute to abnormal fibril growth, evidenced by [describe specific observations].

Various polymorphic fibril types may exhibit distinct diffusion dynamics, influenced by surface heterogeneity.[63–65] For instance, 'helical' fibrils could regulate diffusion rates by altering the orientation of monomers on their surface, such as by modulating sliding speeds, as observed from this work. These micro-level changes might have significant implications at the macroscopic level, possibly affecting the overall rate of fibril growth. A scenario where monomers slide excessively rapidly might be less favorable. Experiments conducted using [technique] have shown how changes in monomer orientation on 'helical' fibrils can alter the overall growth rate of the fibrils, as evidenced by [describe results].

Twisted fibrils could promote slower protein movement, favoring elongation at rates compatible with biological timescales [Citation]. This suggests that the physical structure and surface properties of fibrils are not just passive elements but actively influence the behavior

and movement of amyloid proteins. Such insights could be pivotal in understanding the mechanistic pathways involved in the progression of neurodegenerative diseases.

5 CONCLUSIONS

This study provides critical insights into the role of surface-mediated secondary processes in Alzheimer's disease, particularly in the context of Abeta42 peptide aggregation. Through the use of coarse-grained molecular dynamics simulations, we focused on elucidating the molecular intricacies of these secondary processes, distinct from primary nucleation.

Central to our investigation was the analysis of a freely diffusing Abeta42 monomer in proximity to pre-formed fibril structures. We meticulously calculated the diffusion coefficient (D) of the monomer as it interacted with both straight and twisted fibril surfaces, taking into account different monomer orientations. Our research reveals a strong and consistent correlation between the monomer's diffusion coefficient and its orientation on the fibril surface. This finding is crucial, as it remains valid across different degrees of fibrillar twisting, emphasizing the significance of monomer orientation in surface-mediated secondary aggregation processes.

Additionally, our study delved into the differential effects of fibril surfaces on monomer dynamics. We conducted a comparative analysis of the C-terminal and N-terminal surfaces, observing that monomers exhibit lower diffusion coefficients on the N-terminal surface. This variation in diffusion dynamics is largely attributable to differences in surface roughness, quantified using root-mean-square deviation (RMSD). Such disparities in shape and roughness of the fibril surfaces are pivotal in shaping the monomer dynamics, thereby influencing the secondary aggregation process.

In conclusion, our findings highlight the complex and nuanced role of surface characteristics in the secondary aggregation processes of Abeta42 peptides in Alzheimer's disease. By shedding light on the molecular dynamics of these processes, our study opens new avenues for understanding and potentially intervening in the progression of Alzheimer's disease, focusing on the manipulation of surface-mediated secondary aggregation mechanisms.

Acknowledgement:

This work was supported by the National Science and Technology Council (NSTC), Taiwan, Grant No. 112-2113-M-194-012.

REFERENCES

(1) Hardy, J.; Selkoe, D. J. The Amyloid Hypothesis of Alzheimer's Disease: Progress and Problems on the Road to Therapeutics. *Science* **2002**, *297* (5580), 353–356.

(2) Knopman, D. S.; Jones, D. T.; Greicius, M. D. Failure to Demonstrate Efficacy of Aducanumab: An Analysis of the EMERGE and ENGAGE Trials as Reported by Biogen, December 2019. *Alzheimers. Dement.* **2021**, *17* (4), 696–701.

(3) Center for Drug Evaluation; Research. *FDA's decision to approve new treatment for Alzheimer's disease*. U.S. Food and Drug Administration. https://www.fda.gov/drugs/news-events-human-drugs/fdas-decision-approve-new-treatment-alzheimers-disease (accessed 2023-12-23).

(4) Piller, C. *Second death linked to potential antibody treatment for Alzheimer's disease*. Science News. https://www.science.org/content/article/second-death-linked-potential-antibody-treatment-alzheimer-s-disease?utm_source=sfmc&utm_medium=email&utm_campaign=DailyLatestNews&utm_content=alert&et_rid=504035807&et_cid=4509061.

(5) Bucciantini, M.; Giannoni, E.; Chiti, F.; Baroni, F.; Formigli, L.; Zurdo, J.; Taddei, N.; Ramponi, G.; Dobson, C. M.; Stefani, M. Inherent Toxicity of Aggregates Implies a Common Mechanism for Protein Misfolding Diseases. *Nature* **2002**, *416* (6880), 507–511.

(6) Walsh, D. M.; Klyubin, I.; Fadeeva, J. V.; Cullen, W. K.; Anwyl, R.; Wolfe, M. S.; Rowan, M. J.; Selkoe, D. J. Naturally Secreted Oligomers of Amyloid Beta Protein Potently Inhibit Hippocampal Long-Term Potentiation in Vivo. *Nature* **2002**, *416* (6880), 535–539.

(7) Kayed, R.; Head, E.; Thompson, J. L.; McIntire, T. M.; Milton, S. C.; Cotman, C. W.; Glabe, C. G. Common Structure of Soluble Amyloid Oligomers Implies Common Mechanism of Pathogenesis. *Science* **2003**, *300* (5618), 486–489.

(8) Nguyen, P. H.; Ramamoorthy, A.; Sahoo, B. R.; Zheng, J.; Faller, P.; Straub, J. E.; Dominguez, L.; Shea, J.-E.; Dokholyan, N. V.; De Simone, A.; Ma, B.; Nussinov, R.; Najafi, S.; Ngo, S. T.; Loquet, A.; Chiricotto, M.; Ganguly, P.; McCarty, J.; Li, M. S.; Hall, C.; Wang, Y.; Miller, Y.; Melchionna, S.; Habenstein, B.; Timr, S.; Chen, J.; Hnath, B.; Strodel, B.; Kayed, R.; Lesné, S.; Wei, G.; Sterpone, F.; Doig, A. J.; Derreumaux, P. Amyloid Oligomers: A Joint Experimental/Computational Perspective on Alzheimer's Disease, Parkinson's Disease, Type II Diabetes, and Amyotrophic Lateral Sclerosis. *Chem. Rev.* **2021**, *121* (4), 2545–2647.

(9) Oosawa, F.; Asakura, S. *Thermodynamics of the Polymerization of Protein*; Molecular Biology S.; Academic Press: San Diego, CA, 1975.

(10) Oosawa, F.; Kasai, M. A Theory of Linear and Helical Aggregations of Macromolecules. *J. Mol. Biol.* **1962**, *4*, 10–21.

(11) Lee, J.; Culyba, E. K.; Powers, E. T.; Kelly, J. W. Amyloid-β Forms Fibrils by Nucleated Conformational Conversion of Oligomers. *Nat. Chem. Biol.* **2011**, *7* (9), 602–609.

(12) Knowles, T. P. J.; Waudby, C. A.; Devlin, G. L.; Cohen, S. I. A.; Aguzzi, A.; Vendruscolo, M.; Terentjev, E. M.; Welland, M. E.; Dobson, C. M. An Analytical Solution to the Kinetics of Breakable Filament Assembly. *Science*. 2009, pp 1533–1537. https://doi.org/10.1126/science.1178250.

(13) Cohen, S. I. A.; Linse, S.; Luheshi, L. M.; Hellstrand, E.; White, D. A.; Rajah, L.; Otzen, D. E.; Vendruscolo, M.; Dobson, C. M.; Knowles, T. P. J. Proliferation of Amyloid-β42 Aggregates Occurs through a Secondary Nucleation Mechanism. *Proc. Natl. Acad. Sci. U. S. A.* **2013**, *110* (24), 9758–9763.

(14) Bishop, M. F.; Ferrone, F. A. Kinetics of Nucleation-Controlled Polymerization. A Perturbation Treatment for Use with a Secondary Pathway. *Biophys. J.* **1984**, *46* (5), 631–644.

(15) Ferrone, F. A.; Hofrichter, J.; Eaton, W. A. Kinetics of Sickle Hemoglobin Polymerization. II. A Double Nucleation Mechanism. *J. Mol. Biol.* **1985**, *183* (4), 611–631.

(16) Ruschak, A. M.; Miranker, A. D. Fiber-Dependent Amyloid Formation as Catalysis of an Existing Reaction Pathway. *Proc. Natl. Acad. Sci. U. S. A.* **2007**, *104* (30), 12341–12346.

(17) Arosio, P.; Knowles, T. P. J.; Linse, S. On the Lag Phase in Amyloid Fibril Formation. *Phys.*

Chem. Chem. Phys. **2015**, *17* (12), 7606–7618.
(18) Cohen, S. I. A.; Arosio, P.; Presto, J.; Kurudenkandy, F. R.; Biverstal, H.; Dolfe, L.; Dunning, C.; Yang, X.; Frohm, B.; Vendruscolo, M.; Johansson, J.; Dobson, C. M.; Fisahn, A.; Knowles, T. P. J.; Linse, S. A Molecular Chaperone Breaks the Catalytic Cycle That Generates Toxic Aβ Oligomers. *Nat. Struct. Mol. Biol.* **2015**, *22* (3), 207–213.
(19) Cohen, S. I. A.; Cukalevski, R.; Michaels, T. C. T.; Šarić, A.; Törnquist, M.; Vendruscolo, M.; Dobson, C. M.; Buell, A. K.; Knowles, T. P. J.; Linse, S. Distinct Thermodynamic Signatures of Oligomer Generation in the Aggregation of the Amyloid-β Peptide. *Nat. Chem.* **2018**, *10* (5), 523–531.
(20) Scheidt, T.; Łapińska, U.; Kumita, J. R.; Whiten, D. R.; Klenerman, D.; Wilson, M. R.; Cohen, S. I. A.; Linse, S.; Vendruscolo, M.; Dobson, C. M.; Knowles, T. P. J.; Arosio, P. Secondary Nucleation and Elongation Occur at Different Sites on Alzheimer's Amyloid-β Aggregates. *Science Advances* **2019**, *5* (4), eaau3112.
(21) Cao, Y.; Tang, X.; Yuan, M.; Han, W. Computational Studies of Protein Aggregation Mediated by Amyloid: Fibril Elongation and Secondary Nucleation. *Prog. Mol. Biol. Transl. Sci.* **2020**, *170*, 461–504.
(22) Törnquist, M.; Michaels, T. C. T.; Sanagavarapu, K.; Yang, X.; Meisl, G.; Cohen, S. I. A.; Knowles, T. P. J.; Linse, S. Secondary Nucleation in Amyloid Formation. *Chem. Commun.* **2018**, *54* (63), 8667–8684.
(23) Wang, Q.; Shah, N.; Zhao, J.; Wang, C.; Zhao, C.; Liu, L.; Li, L.; Zhou, F.; Zheng, J. Structural, Morphological, and Kinetic Studies of β-Amyloid Peptide Aggregation on Self-Assembled Monolayers. *Phys. Chem. Chem. Phys.* **2011**, *13* (33), 15200–15210.
(24) Zhao, J.; Wang, Q.; Liang, G.; Zheng, J. Molecular Dynamics Simulations of Low-Ordered Alzheimer β-Amyloid Oligomers from Dimer to Hexamer on Self-Assembled Monolayers. *Langmuir* **2011**, *27* (24), 14876–14887.
(25) Auer, S.; Trovato, A.; Vendruscolo, M. A Condensation-Ordering Mechanism in Nanoparticle-Catalyzed Peptide Aggregation. *PLoS Comput. Biol.* **2009**, *5* (8), e1000458.
(26) Vácha, R.; Frenkel, D. Relation between Molecular Shape and the Morphology of Self-Assembling Aggregates: A Simulation Study. *Biophys. J.* **2011**, *101* (6), 1432–1439.
(27) Morriss-Andrews, A.; Shea, J.-E. Kinetic Pathways to Peptide Aggregation on Surfaces: The Effects of β-Sheet Propensity and Surface Attraction. *J. Chem. Phys.* **2012**, *136* (6), 065103.
(28) Vácha, R.; Linse, S.; Lund, M. Surface Effects on Aggregation Kinetics of Amyloidogenic Peptides. *J. Am. Chem. Soc.* **2014**, *136* (33), 11776–11782.
(29) Do, T. D.; LaPointe, N. E.; Nelson, R.; Krotee, P.; Hayden, E. Y.; Ulrich, B.; Quan, S.; Feinstein, S. C.; Teplow, D. B.; Eisenberg, D.; Shea, J.-E.; Bowers, M. T. Amyloid β-Protein C-Terminal Fragments: Formation of Cylindrins and β-Barrels. *J. Am. Chem. Soc.* **2016**, *138* (2), 549–557.
(30) Shen, L.; Adachi, T.; Vanden Bout, D.; Zhu, X.-Y. A Mobile Precursor Determines Amyloid-β Peptide Fibril Formation at Interfaces. *J. Am. Chem. Soc.* **2012**, *134* (34), 14172–14178.
(31) Radic, S.; Davis, T. P.; Ke, P. C.; Ding, F. Contrasting Effects of Nanoparticle-Protein Attraction on Amyloid Aggregation. *RSC Adv.* **2015**, *5* (127), 105498.
(32) Shezad, K.; Zhang, K.; Hussain, M.; Dong, H.; He, C.; Gong, X.; Xie, X.; Zhu, J.; Shen, L. Surface Roughness Modulates Diffusion and Fibrillation of Amyloid-β Peptide. *Langmuir* **2016**, *32* (32), 8238–8244.
(33) Lin, Y.-C.; Li, C.; Fakhraai, Z. Kinetics of Surface-Mediated Fibrillization of Amyloid-β (12–28) Peptides. *Langmuir* **2018**, *34* (15), 4665–4672.
(34) Šarić, A.; Buell, A. K.; Meisl, G.; Michaels, T. C. T.; Dobson, C. M.; Linse, S.; Knowles, T. P. J.; Frenkel, D. Physical Determinants of the Self-Replication of Protein Fibrils. *Nat. Phys.* **2016**, *12* (9), 874–880.
(35) Gudowska-Nowak, E.; Oliveira, F. A.; Wio, H. S. Editorial: The Fluctuation-Dissipation Theorem Today. *Frontiers in Physics* **2022**, *10*. https://doi.org/10.3389/fphy.2022.859799.
(36) Milo, R.; Phillips, R. *Cell Biology by the Numbers*; Garland Science, 2015.
(37) Lu, W.; Bueno, C.; Schafer, N. P.; Moller, J.; Jin, S.; Chen, X.; Chen, M.; Gu, X.; Davtyan, A.; de Pablo, J. J.; Wolynes, P. G. OpenAWSEM with Open3SPN2: A Fast, Flexible, and Accessible Framework for Large-Scale Coarse-Grained Biomolecular Simulations. *PLoS Comput. Biol.* **2021**, *17* (2), e1008308.

(38) Ma, Y.-W.; Lin, T.-Y.; Tsai, M.-Y. Fibril Surface-Dependent Amyloid Precursors Revealed by Coarse-Grained Molecular Dynamics Simulation. *Front Mol Biosci* **2021**, *8*, 719320.
(39) Chen, W.; Lu, W.; Wolynes, P. G.; Komives, E. A. Single-Molecule Conformational Dynamics of a Transcription Factor Reveals a Continuum of Binding Modes Controlling Association and Dissociation. *Nucleic Acids Res.* **2021**, *49* (19), 11211–11223.
(40) Jin, S.; Bueno, C.; Lu, W.; Wang, Q.; Chen, M.; Chen, X.; Wolynes, P. G.; Gao, Y. Computationally Exploring the Mechanism of Bacteriophage T7 gp4 Helicase Translocating along ssDNA. *Proc. Natl. Acad. Sci. U. S. A.* **2022**, *119* (32), e2202239119.
(41) Chen, X.; Lu, W.; Tsai, M.-Y.; Jin, S.; Wolynes, P. G. Exploring the Folding Energy Landscapes of Heme Proteins Using a Hybrid AWSEM-Heme Model. *J. Biol. Phys.* **2022**. https://doi.org/10.1007/s10867-021-09596-3.
(42) Eastman, P.; Swails, J.; Chodera, J. D.; McGibbon, R. T.; Zhao, Y.; Beauchamp, K. A.; Wang, L.-P.; Simmonett, A. C.; Harrigan, M. P.; Stern, C. D.; Wiewiora, R. P.; Brooks, B. R.; Pande, V. S. OpenMM 7: Rapid Development of High Performance Algorithms for Molecular Dynamics. *PLOS Computational Biology*. 2017, p e1005659. https://doi.org/10.1371/journal.pcbi.1005659.
(43) Davtyan, A.; Schafer, N. P.; Zheng, W.; Clementi, C.; Wolynes, P. G.; Papoian, G. A. AWSEM-MD: Protein Structure Prediction Using Coarse-Grained Physical Potentials and Bioinformatically Based Local Structure Biasing. *J. Phys. Chem. B* **2012**, *116* (29), 8494–8503.
(44) Tsai, M.-Y.; Zheng, W.; Balamurugan, D.; Schafer, N. P.; Kim, B. L.; Cheung, M. S.; Wolynes, P. G. Electrostatics, Structure Prediction, and the Energy Landscapes for Protein Folding and Binding. *Protein Sci.* **2016**, *25* (1), 255–269.
(45) Sirovetz, B. J.; Schafer, N. P.; Wolynes, P. G. Protein Structure Prediction: Making AWSEM AWSEM-ER by Adding Evolutionary Restraints. *Proteins* **2017**, *85* (11), 2127–2142.
(46) Chen, M.; Lin, X.; Lu, W.; Schafer, N. P.; Onuchic, J. N.; Wolynes, P. G. Template-Guided Protein Structure Prediction and Refinement Using Optimized Folding Landscape Force Fields. *J. Chem. Theory Comput.* **2018**, *14* (11), 6102–6116.
(47) Zheng, W.; Tsai, M.-Y.; Chen, M.; Wolynes, P. G. Exploring the Aggregation Free Energy Landscape of the Amyloid-β Protein (1-40). *Proc. Natl. Acad. Sci. U. S. A.* **2016**, *113* (42), 11835–11840.
(48) Zheng, W.; Tsai, M.-Y.; Wolynes, P. G. Comparing the Aggregation Free Energy Landscapes of Amyloid Beta(1-42) and Amyloid Beta(1-40). *J. Am. Chem. Soc.* **2017**, *139* (46), 16666–16676.
(49) Tsai, M.-Y.; Zhang, B.; Zheng, W.; Wolynes, P. G. Molecular Mechanism of Facilitated Dissociation of Fis Protein from DNA. *J. Am. Chem. Soc.* **2016**, *138* (41), 13497−13500.
(50) Tsai, M.-Y.; Zheng, W.; Chen, M.; Wolynes, P. G. Multiple Binding Configurations of Fis Protein Pairs on DNA: Facilitated Dissociation versus Cooperative Dissociation. *J. Am. Chem. Soc.* **2019**, *141* (45), 18113–18126.
(51) Potoyan, D. A.; Zheng, W.; Komives, E. A.; Wolynes, P. G. Molecular Stripping in the NF-κB/IκB/DNA Genetic Regulatory Network. *Proc. Natl. Acad. Sci. U. S. A.* **2016**, *113* (1), 110–115.
(52) Zhang, B.; Zheng, W.; Papoian, G. A.; Wolynes, P. G. Exploring the Free Energy Landscape of Nucleosomes. *J. Am. Chem. Soc.* **2016**, *138* (26), 8126–8133.
(53) Jin, S.; Contessoto, V. G.; Chen, M.; Schafer, N. P.; Lu, W.; Chen, X.; Bueno, C.; Hajitaheri, A.; Sirovetz, B. J.; Davtyan, A.; Papoian, G. A.; Tsai, M.-Y.; Wolynes, P. G. AWSEM-Suite: A Protein Structure Prediction Server Based on Template-Guided, Coevolutionary-Enhanced Optimized Folding Landscapes. *Nucleic Acids Res.* **2020**, *48* (W1), W25–W30.
(54) Smaoui, M. R.; Poitevin, F.; Delarue, M.; Koehl, P.; Orland, H.; Waldispühl, J. Computational Assembly of Polymorphic Amyloid Fibrils Reveals Stable Aggregates. *Biophys. J.* **2013**, *104* (3), 683–693.
(55) Cecchini, M.; Rao, F.; Seeber, M.; Caflisch, A. Replica Exchange Molecular Dynamics Simulations of Amyloid Peptide Aggregation. *J. Chem. Phys.* **2004**, *121* (21), 10748–10756.
(56) Schwierz, N.; Frost, C. V.; Geissler, P. L.; Zacharias, M. From Aβ Filament to Fibril: Molecular Mechanism of Surface-Activated Secondary Nucleation from All-Atom MD Simulations. *J. Phys. Chem. B* **2017**, *121* (4), 671–682.
(57) Lin, T.-Y.; Ma, Y.-W.; Tsai, M.-Y. Early-Stage Oligomerization of Prion-like Polypeptides Reveals the Molecular Mechanism of Amyloid-Disrupting Capacity by Proline Residues. *J.*

Phys. Chem. B **2023**, *127* (5), 1074–1088.
(58) Charest, N.; Tro, M.; Bowers, M. T.; Shea, J.-E. Latent Models of Molecular Dynamics Data: Automatic Order Parameter Generation for Peptide Fibrillization. *J. Phys. Chem. B* **2020**, *124* (37), 8012–8022.
(59) Kumar, S.; Rosenberg, J. M.; Bouzida, D.; Swendsen, R. H.; Kollman, P. A. THE Weighted Histogram Analysis Method for Free-Energy Calculations on Biomolecules. I. The Method. *Journal of Computational Chemistry*. 1992, pp 1011–1021. https://doi.org/10.1002/jcc.540130812.
(60) Scherer, M. K.; Trendelkamp-Schroer, B.; Paul, F.; Pérez-Hernández, G.; Hoffmann, M.; Plattner, N.; Wehmeyer, C.; Prinz, J.-H.; Noé, F. PyEMMA 2: A Software Package for Estimation, Validation, and Analysis of Markov Models. *J. Chem. Theory Comput.* **2015**, *11* (11), 5525–5542.
(61) Thacker, D.; Barghouth, M.; Bless, M.; Zhang, E.; Linse, S. Direct Observation of Secondary Nucleation along the Fibril Surface of the Amyloid β 42 Peptide. *Proc. Natl. Acad. Sci. U. S. A.* **2023**, *120* (25), e2220664120.
(62) Jean, L.; Lee, C. F.; Vaux, D. J. Enrichment of Amyloidogenesis at an Air-Water Interface. *Biophys. J.* **2012**, *102* (5), 1154–1162.
(63) Bouchard, M.; Zurdo, J.; Nettleton, E. J.; Dobson, C. M.; Robinson, C. V. Formation of Insulin Amyloid Fibrils Followed by FTIR Simultaneously with CD and Electron Microscopy. *Protein Sci.* **2000**, *9* (10), 1960–1967.
(64) Kurouski, D.; Dukor, R. K.; Lu, X.; Nafie, L. A.; Lednev, I. K. Normal and Reversed Supramolecular Chirality of Insulin Fibrils Probed by Vibrational Circular Dichroism at the Protofilament Level of Fibril Structure. *Biophys. J.* **2012**, *103* (3), 522–531.
(65) Usov, I.; Adamcik, J.; Mezzenga, R. Polymorphism Complexity and Handedness Inversion in Serum Albumin Amyloid Fibrils. *ACS Nano* **2013**, *7* (12), 10465–10474.